Tight Binding Simulation of Quantum Electron Transport in Type II Resonant Tunneling Devices

Matsuto Ogawa, Takashi Sugano, and Tanroku Miyoshi

Department of Electrical and Electronics Engineering
Kobe University, 1 Rokkodai, Nada, Kobe 657-8501, Japan
Phone & Facsimile: +81-78-803-1070
E-mail: ogawa@eedept.kobe-u.ac.jp

We report on calculations of quantum transport in an InAs/GaSb/AlSb (type II) based double barrier resonant tunneling diode. Our procedure uses a realistic band structure based on an empirical tight binding theory. In the formulation, an evanescent-wave matching at heterointerfaces as well as the conduction and valence-band-mixing effects, in addition, space charge effect are duly taken into account. Comparison has been made between our results and calculations using a two-band model which considers only the lowest conduction and the light-hole states. Our results show that current-voltage characteristics have extra current peak due to significant heavy-hole mixing effects in the GaSb quantum well. It should be also noted that the matching of evanescent electron modes is essentially necessary to include the valley-mixing effects for the heterostructures, since breaking of a lattice-translational symmetry occurs at the interfaces.

1. Introduction

The InAs/GaSb (InAs/AlSb/GaSb) type II heterostructures have been attracting much attention, since they have led to demonstration of several novel devices, specifically double barrier resonant tunneling diodes (DBRTDs) with high peak-to-valley current ratios (PVRs) [1-3]. In such structures, the interaction between the conduction electrons and the valence band holes is important, since the impinging electron from the InAs enters the valence band of the GaSb side. In order to simulate such interaction realistically, we have to include properly the full band structure effect such as the band-mixing effect among the conduction, the heavy-hole (HH) and light-hole (LH) bands, in addition, the nonparabolicity. To date, only the multiband treatment [4] or a simple two-band model [5] have been applied to analyze quantum transport in single barrier diodes for simplicity and saving computational costs.

In this paper, we present calculations of quantum electron transport in an InAs/AlSb/GaSb type II DBRTD based on an empirical tight-binding calculation. In Sec. 2 we briefly illustrate the complex band structures and evanescent electron modes in the materials. Section 3 presents our numerical results and Sec. 4 our conclusions.

0-7803-4369-7/98 $10.00

2. Evanescent States in Type II Heterostructures

We consider carrier transport in [0 0 1] direction in zinc-blende crystals. We employ an empirical tight-binding (TB) model [7] with a basis of five orbitals per atom (s, p_x, p_y, p_z, s^*) with spins assuming nearest neighbor overlaps, where s^* implies an excited s-state which includes the interaction from inner shells.

We express the total electron wave function in terms of the Bloch sum of the anion (a) and cation (c) states as

$$|\Psi(k_z, \boldsymbol{k}_\parallel, z)\rangle = \sum_{\sigma,\alpha^a,\alpha^c} \left[C_{\sigma\alpha^a}(k_z)|\boldsymbol{k}_\parallel, \sigma, \alpha^a\rangle + C_{\sigma\alpha^c}(k_z)|\boldsymbol{k}_\parallel, \sigma, \alpha^c\rangle\right], \quad (1)$$

where

$$|\boldsymbol{k}_\parallel, \sigma, \alpha^a\rangle = \frac{1}{\sqrt{N_\parallel}} \sum_{\boldsymbol{R}_\parallel} \exp(i\boldsymbol{k}_\parallel \cdot \boldsymbol{R}_\parallel) |\boldsymbol{R}_\parallel, \sigma, \alpha^a\rangle,$$
$$|\boldsymbol{k}_\parallel, \sigma, \alpha^c\rangle = \frac{1}{\sqrt{N_\parallel}} \sum_{\boldsymbol{R}_\parallel} \exp\left[i\boldsymbol{k}_\parallel \cdot (\boldsymbol{R}_\parallel + \boldsymbol{v})\right] |\boldsymbol{R}_\parallel + \boldsymbol{v}, \sigma, \alpha^c\rangle. \quad (2)$$

Here $|\boldsymbol{k}_{\|}, \sigma, \alpha^j\rangle$ denotes a Bloch sum of α^j-like ($j = a, c$) atomic orbitals including spin index associated with the in-plane wave vector $\boldsymbol{k}_{\|}$, k_z the wave vector in propagating direction, σ labels the index of the layer comprised of both the anion and cation atoms, $N_{\|}$ total lattice points in x-y plane, and $\boldsymbol{R}_{\|}$ is the lattice position vector in x-y plane. In eq. (2), $\boldsymbol{v}$ is the basis vector of a unit cell, that is, $\boldsymbol{v} = a(\boldsymbol{x} + \boldsymbol{y} + \boldsymbol{z})/4$, where a is the lattice constant (see Fig.1).

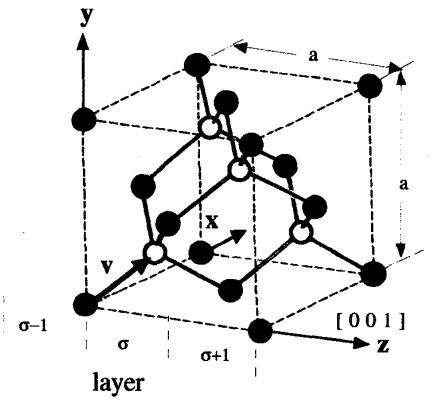

Fig. 1 Location of anion atom (open circle) and cation atom (closed circle) in a Zinc Blende crystal. Each layer σ is defined as a monolayer comprised of anion/cation atomic plane in [0 0 1] direction.

We substitute $|\Psi(k_z, \boldsymbol{k}_{\|}, z)\rangle$ into the Schrödinger equation $(H - E)\,|\Psi(k_z, \boldsymbol{k}_{\|}, z)\rangle = 0$, where H is the Hamiltonian for the crystal and E is the electron energy. Projecting the resulting equation in atomic orbitals located at atomic layer σ, we can relate the coefficients in layer σ to those in layer $\sigma \pm 1$ with the aid of a transfer matrix as

$$T\boldsymbol{C} = \exp(ik_z z)\,\boldsymbol{C}, \tag{3}$$

where

$$T \equiv T_c T_a, \tag{4}$$

$$T_j = \begin{pmatrix} -[H^{(+)}(\sigma)]^{-1} H^{(0)}(\sigma) & -[H^{(+)}(\sigma)]^{-1} H^{(-)}(\sigma) \\ 1 & 0 \end{pmatrix} \quad (j = a, c), \tag{5}$$

and $\boldsymbol{C}$ is coefficient vector comprised of $C_{\sigma\alpha^j}$, and $H^{(+)}$,$H^{(0)}$, and $H^{(-)}$ are matrices with the matrix elements:

$$\begin{aligned} H^{(+)}(\sigma)_{\alpha^j\alpha'^j} &= \langle \boldsymbol{k}_{\|}, \sigma, \alpha^j | H | \boldsymbol{k}_{\|}, \sigma + 1, \alpha'^j \rangle, \\ H^{(0)}(\sigma)_{\alpha^j\alpha'^j} &= \langle \boldsymbol{k}_{\|}, \sigma, \alpha^j | H | \boldsymbol{k}_{\|}, \sigma, \alpha'^j \rangle \\ &\quad - E\delta_{\alpha^j\alpha'^j}, \\ H^{(-)}(\sigma)_{\alpha^j\alpha'^j} &= \langle \boldsymbol{k}_{\|}, \sigma, \alpha^j | H | \boldsymbol{k}_{\|}, \sigma - 1, \alpha'^j \rangle. \end{aligned} \tag{6}$$

Since the transfer matrix T is a function of E, the eigenvalue equation (3) yields the E-k_z energy band diagram.

The calculated band structures of InAs, GaSb bulk at $\boldsymbol{k}_{\|} = \boldsymbol{0}$ in the [0 0 1] direction are shown in Fig. 2 (a) and (b), respectively.

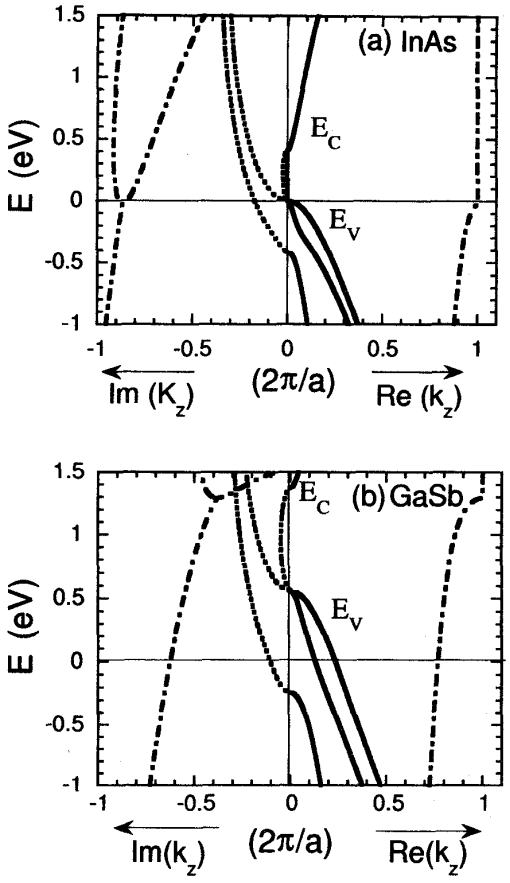

Fig. 2 Complex band structures of (a) InAs bulk and (b) GaSb bulk along the [100] direction. Both the real bands (solid lines: **Im** $k_z = 0$) and the complex bands corresponding to evanescent modes (dashed lines: **Re** $k_z \neq 0$ and **Im** $k_z \neq 0$) are shown. The origin of the electron energy is set at the valence-band top of InAs.

In the calculation we have used the typical empirical tight-binding parameters[6]. It should be noted that the eigenvalue equation (3) gives both real and complex solutions or evanescent modes of k_z. The real k_z produces the Bloch states (solid lines) and the complex k_z (dashed lines=pure imaginary states: **Re** $k_z = 0$, **Im** $k_z \neq 0$ and the pairs of dotted dashed lines: **Re** $k_z \neq 0$, **Im** $k_z \neq 0$) produces the evanescent states which grow or decay in z direction. At a heterointerface such as a InAs/GaSb heterojunction, where the translational symmetry in z direction is lacking, these evanescent modes must be taken into account to match the impinging electron waves to the propagating waves into the other side. In addition, we have to note that both the real LH and HH dispersion

curves of GaSb show significant non-parabolicity, which cannot be expressed by a simple 2-band model with effective masses.

We use the solutions to analyze quantum transport in a InAs/GaSb/AlSb DBRTD fabricated on (0 0 1) InAs whose model will be shown in Fig. 3. We reorder the bulk states impinging from the left electrode (L) so that the first 10 states ($j = 1, \cdots, 10$) correspond to states which propagate or decay in $+z$ direction, while last 10 states ($j = 11, \cdots, 20$) correspond to those propagating or decaying in $-z$ direction. Note that we have 20 states because we have included spin indices in the atomic orbitals. The boundary conditions at the L and right (R) electrodes are given using these reordered bulk states[4]

$$|\Psi; L\rangle = \sum_{j=1}^{10} \left(I_j |k_z^j; L\rangle + r_j |k_z^{j+10}; L\rangle \right) \quad (7)$$

$$|\Psi; R\rangle = \sum_{j=1}^{10} t_j |k_z^j; R\rangle, \quad (8)$$

where $|k_z^j; L\rangle$ and $|k_z^j; R\rangle$ are the reordered bulk states in the L, and R electrodes, respectively, I_j amplitude of the incident mode, r_j that of the reflected mode, and t_j is that of the transfer mode. We can relate these incident amplitudes to the coefficient vector $\boldsymbol{C}$ in the neighboring layer using the transfer matrix T as shown in eq. (3) and repeat this process until the layer reaches to the right electrode R. At the heterointerface, the transfer method duly includes the matching condition of the evanescent modes as well as the real modes.

The transmission coefficient (transmissivity) for electron impinging from L and propagating to R is given by

$$T^{L \to R}(E, \boldsymbol{k}_{\|}) = \sum_{j=1}^{10} |t_j(E, \boldsymbol{k}_{\|})|^2 \frac{|\partial E_j / \partial k_z^j|}{|\partial E_I / \partial k_z|}, \quad (9)$$

where E_I, and E_j are the incident energy and transmitted energy, respectively, defined as

$$E_j = E(k_z^j) + E(\boldsymbol{k}_{\|}). \quad (10)$$

In the above equation, in-plane non-parabolicity of the band structure is taken into account in the second term.

The tunneling current is given by the following expression :

$$J = \frac{2e}{(2\pi)^2 \hbar} \int_0^{\infty} k_{\|} dk_{\|} \int_0^{\infty} dE \, T(E, k_{\|}, V) \left[f_E(E) - f_C(E) \right], \quad (11)$$

where f_E and f_C are the Fermi-Dirac distribution functions at the emitter and collector, respectively, and V is the applied bias voltage. This equation is slightly different from the conventional tunneling current formula[9], since we have included the in-plane non-parabolicity in the transmissivity $T(E, k_{\|}, V)$.

The potential profile is calculated by solving the Poisson equation. In the equation the charge term is composed of donors and the electrons. We assume that the electron concentration obeys the Thomas-Fermi (T-F) theory, that is, it is given by

$$n(z) = \frac{(2m^*(z))^{3/2}}{2\pi^2 \hbar^3} \int_0^{\infty} \frac{\sqrt{E} dE}{1 + \exp\left(\frac{E_c(z) + E - E_F}{k_B T} \right)} \quad (12)$$

with assuming a parabolic conduction band in z direction. Although we must use the correct form of electron concentration (eq.(16) of [8]) for self-consistent calculation, we have used the T-F model in this paper for the sake of simplicity, since we are interested in the effect of the band-mixing and the existence of the evanescent modes on the transport properties.

3. Numerical Results

We study quantum transport in a InAs/AlSb/GaSb DBRTD fabricated on (0 0 1) InAs as illustrated in Fig. 3. The structure has a GaSb well of 14 monolayers (ML) and surrounded by double undoped AlSb barrier of 6 monolayers, and an InAs emitter and collector electrode each doped with $N_D = 10^{17}$ cm^{-3}. We have assumed that the InAs, AlSb, and GaSb lattice constants are nearly same (1 ML $\approx$ 0.30 nm) and ignored possible existence of strain among those layers[10]. The device temperature T is assumed to be 77 K.

Figure 3 also shows both the band structure and carrier concentration profile at the bias of 0.2 V. Since we have adopted the T-F model for the carrier concentration, it shows maximum at the left InAs/AlSb heterointerface and abruptly decreases in the barrier and the well region and then gradually increases toward the collector region as shown in the figure.

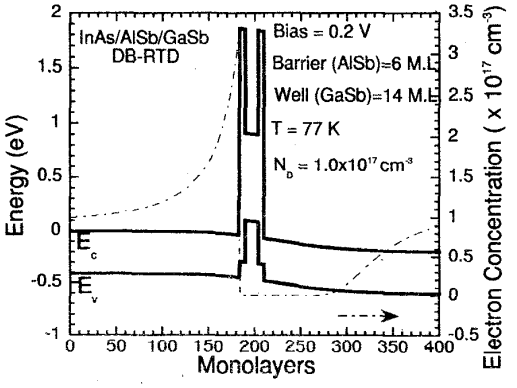

Fig. 3 Schematic structure of a InAs/AlSb/GaSb (n-i-n) double barrier resonant tunneling diode at 0.2 V bias.

Figure 4 (a) shows I-V characteristics of the DBRTD calculated by the present TB model (solid line) and the 2-band model (dashed line) where space charge effects

are taken into account. In the 2-band model, we have assumed there exist only parabolic conduction band (CB) of InAs and lowest LH state of GaSb well in each region and no interaction between the LH and the HH bands in the well.

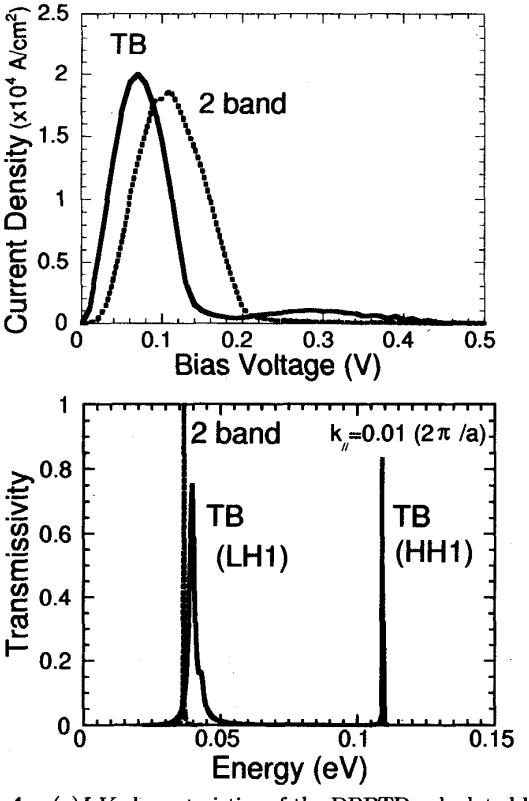

Fig. 4 (a)*I-V* characteristics of the DBRTD calculated by the tight-binding (TB) model (solid line) and the two-band model (dashed line). (b)Calculated transmissivity of carriers as a function of incident energy; solid line = TB model and dashed line = two-band model.

The first peak in the *I-V* curve is mainly due to the electron tunneling from the conduction band of InAs emitter to the LH state in the GaSb well. However, it should be emphasized that the second peak arises from the HH tunneling which cannot be explained by the conventional 2-band model[4]. The transmission probability (transmissivity) of carriers at $k_{\|} = 0.01 \cdot 2\pi/a$ is shown in Fig.4 (b). Transmissivity calculated by the TB model exhibits a HH resonance which is not present in the 2-band model. This situation is same for any $k_{\|}$. The enhanced transmissivity of HH states is due to the band-mixing effects between HH and LH state in the valence band, which can be duly included by the multiband treatment as stated in Sec.2. In addition, the LH resonance (first peak) calculated by the TB model is wider than that of 2-band model. This result indicates that the coupling between InAs CB state and GaSb LH state is weaker than that predicted by the 2-band model. Although the PVRs of type II RTDs are better than that of GaAs/Al(Ga)As devices [1-3], the HH interaction in the valence band may have a crucial effect in the device performance of InAs/AlSb/GaSb DBRTDs.

4. Conclusion

We have studied a InAs/AlSb/GaSb type II DBRTD based on the multiband TB simulation where an evanescent-wave matching at heterointerfaces as well as the conduction and valence-band-mixing effects, in addition, space charge effect are taken into account.

We have calculated *I-V* characteristics compared with conventional 2-band model. As a result, it is shown that in the InAs/AlSb/GaSb DBRTD the heavy-hole states have the significant role in the tunneling processes.

To include possible effect of carrier scattering such as LO phonon scattering *etc.* for quantitative comparison with experimental data, we can extend our method with the aid of the non-equilibrium Green function formalism [11,12].

References

1. L. F. Luo, R. Beresford, and W. I. Wang, Appl. Phys. Lett. **53**, (1988) 2320.
2. J. R. Söderström, E. R. Brown, C. D. Parker, L. .J. Mahoney, J. Y. Yao, T. .G. Andersson, and T. C. McGill, Appl. Phys. Lett. **58** (1991) 275.
3. R. E. Carnahan, M. A. Maldonado, K.P. Martin, A. Nogaret, R.J. Higgins, L.A. Cury, D.K. Maude, J.C. Portal, J.F. Chen, and A.Y. Cho, Appl. Phys. Lett. **62** (1993) 1385.
4. D. Z. -Y. Ting, E. T. Yu, and T. C. McGill, Phys. Rev. B**45** (1992) 3583.
5. R. Q. Yang and J. M. Xu, J. Appl. Phys. **72** (1992) 4714.
6. P. Vogl, H. P. Hyalmarson, and J. D. Dow, J. Phys. Chem. Solids, **44** (1983) 365.
7. J. C. Slater and G. F. Koster, Phys. Rev. **94** 1498 (1954) 1498.
8. M. Ogawa, T. Sugano, and T. Miyoshi, Solid St. Electron. **42** (1998) 1527.
9. R. Tsu and L. Esaki, Appl. Phys. Lett. **22** (1973) 562.
10. T. B. Boykin, R. E. Carnahan, and R. J. Higgins, Phys. Rev. B**48** (1993) 14232.
11. M. A. Davidovich, E. V. Anda, C. Tejedor, and G. Platero, Phys. Rev. B**47** (1993) 4475.
12. R. Lake , G. Klimeck, R.C. Bowen, and D. Jovanovic J. Appl. Phys. **81** (1997) 7845.